THE GEOLOGICAL SOCIETY OF AMERICA®

Asymmetric exhumation of the Mount Everest region: Implications for the tectono-topographic evolution of the Himalaya

B. Carrapa[1], X. Robert[2,3], P.G. DeCelles[1], D.A. Orme[1,4], S.N. Thomson[1], and L.M. Schoenbohm[5]
[1]Department of Geosciences, University of Arizona, Tucson, Arizona 85721, USA
[2]Institut des Sciences de la Terre, Université Joseph Fourier, CNRS, F-38041 Grenoble Cedex 9, France
[3]Université Grenoble Alpes, CNRS, IRD, IFSTTAR, ISTerre, F-38000 Grenoble Cedex 9, France
[4]Department of Geological Sciences, Stanford University, Stanford, California 94305, USA
[5]Department of Earth Sciences, University of Toronto, Toronto, Ontario M5S 3B1, Canada

ABSTRACT

The tectonic and topographic history of the Himalaya-Tibet orogenic system remains controversial, with several competing models that predict different exhumation histories. Here, we present new low-temperature thermochronological data from the Mount Everest region, which, combined with thermal-kinematic landscape evolution modeling, indicate asymmetric exhumation of Mount Everest consistent with a scenario in which the southern edge of the Tibetan Plateau was located >100 km farther south during the mid-Miocene. Northward plateau retreat was caused by erosional incision during the Pliocene. Our results suggest that the South Tibetan Detachment was a localized structure and that no coupling between precipitation and erosion is required for Miocene exhumation of Greater Himalayan Sequence rocks on Mount Everest.

INTRODUCTION

Mount Everest is the culmination of the High Himalayan topographic crest, which forms the boundary between the arid Tibetan Plateau and the more rugged and humid southern side of the Himalaya (Fig. 1). Although much work has been done on the middle to late Cenozoic tectonic history of Greater Himalaya Sequence (GHS) midcrustal rocks in the Mount Everest region (e.g., Murphy and Harrison, 1999; Cottle et al., 2015), the timing and magnitude of exhumation of these rocks remain largely unresolved. Also, the development of Himalayan topography is uncertain: Does the modern topography represent the culmination of southward growth of Tibet, or northward erosional retreat of the plateau?

The exhumation history of GHS rocks with respect to the South Tibetan Detachment System (STDS) is important for testing tectonic models for the Himalaya. The STDS has been interpreted as a gravity-driven normal fault (Burg et al., 1984; Pêcher, 1991), the northern boundary of an extruded wedge of GHS rocks (Burchfiel et al., 1992), the top of a midcrustal ductile channel (Beaumont et al., 2004; Jamieson et al., 2004), and a passive roof thrust above a southward-verging wedge of GHS rocks (Yin, 2006). These models make different predictions for the exhumation history of GHS rocks.

Thermochronological data are sparse and mostly available for the southern side of the High Himalaya (e.g., Thiede and Ehlers, 2013, and references therein). Here, we present new white mica $^{40}Ar/^{39}Ar$, apatite fission-track (AFT), and apatite (U-Th)/He (AHe) thermochronological data, which, when combined with existing data, can test these models. We couple this with numerical modeling to constrain the north-to-south tectono-topographic and exhumation history across the highest part of the Himalaya.

GEOLOGICAL SETTING OF MOUNT EVEREST

The Himalayan thrust belt is composed of upper-crustal rocks that have been thrust southward since early Cenozoic time. The northernmost major thrust fault in the range is the Main Central Thrust (MCT), which places amphibolite-grade GHS rocks on top of Lesser Himalayan low-grade metasedimentary rocks (Fig. 1). The most significant structure in the Mount Everest region is the northward-dipping STDS, which separates rocks of the Tethyan Himalayan sequence (THS) above from the GHS below (Figs. 1B and 1C; Burchfiel et al., 1992; Burg et al., 1984). The THS consists of Paleozoic–Mesozoic sedimentary and low-grade metasedimentary rocks that were incorporated into the Himalayan orogenic wedge during Eocene and Oligocene time (Aikman et al., 2008) and buried GHS protoliths to depths sufficient for Barrovian metamorphism. The GHS was subsequently exhumed and thrust southward on top of Lesser Himalayan rocks along the MCT during early Miocene time (e.g., Hodges, 2000). Cenozoic leucogranites are common in GHS rocks and formed by decompression anatexis of metapelites and gneisses during STDS slip (e.g., Harris and Massey, 1994), mostly between ca. 22 and 12 Ma (e.g., Cottle et al., 2015, and references therein).

CLIMATE ACROSS MOUNT EVEREST

The Himalaya constitutes an orographic barrier to northward movement of southerly air masses; the result is a sharp gradient in precipitation, with rainfall of 1–3 m/yr south of the divide and <0.5 m north of the divide (Bookhagen and Burbank, 2006). Mount Everest is flanked on the south and east by the steep Khumbu and Kangshung Glaciers, and to the north by the less-steep East Rongbuk and West Rongbuk Glaciers (Fig. 2A). The Khumbu and Kangshung Glacier headwalls truncate the West Rongbuk and East Rongbuk Glacier headwalls, respectively (Fig. 2A), indicating the importance of headward glacial erosion south of the divide (Scherler et al., 2011). Advances of the Rongbuk and Khumbu Glaciers were broadly synchronous and correspond to times of Holocene strengthened monsoon precipitation (Owen et al., 2009).

THERMOCHRONOLOGICAL RESULTS FROM MOUNT EVEREST

We collected samples from the Rongbuk and Gyachung Chhu Rivers draining the northern flank of Mount Everest and neighboring summits (Fig. 2) and 12 samples of GHS gneiss and leucogranite in the footwall of the STDS along the eastern wall of Rongbuk Gorge (Fig. 2) for AFT, AHe, and white mica $^{40}Ar/^{39}Ar$ thermochronology (see the GSA Data Repository[1]). The detrital data set provides the first catchment-wide exhumation record for the Mount Everest region. Seven of the bedrock samples produced AFT ages, and one sample was analyzed for AHe thermochronology (Table DR1 in the GSA Data Repository). The combination of dated minerals constrains the cooling history of these

[1]GSA Data Repository item 2016198, analytical information and data tables, is available online at www.geosociety.org/pubs/ft2016.htm, or on request from editing@geosociety.org.

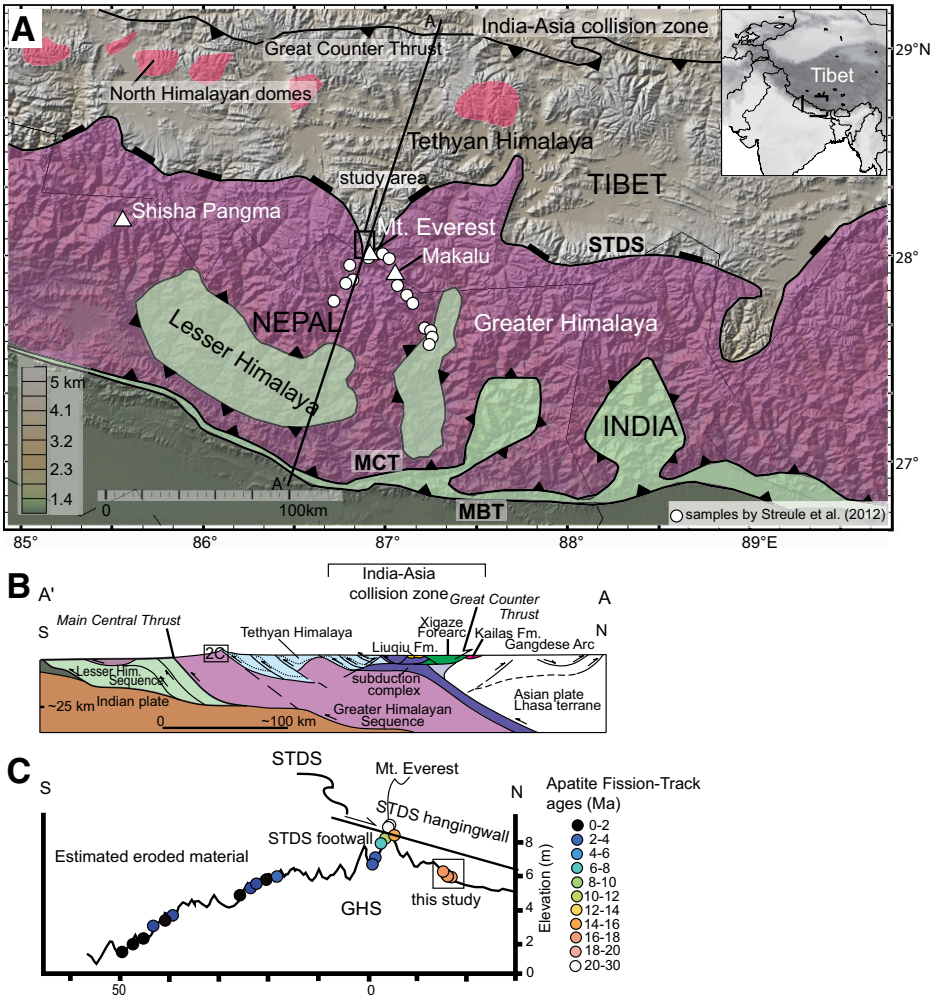

Figure 1. A: Simplified digital elevation model of Asia and geological map of central Himalaya and southern Tibet, modified from Yin (2006); inset shows broader geographic context. B: Schematic north-south cross section of central Himalayan thrust belt, modified from Murphy (2007). C: Topographic profile across Mount Everest with locations of samples from this study, Streule et al. (2012), and Sakai et al. (2005). MCT—Main Central Thrust; MBT—Main Boundary Thrust; STDS—South Tibetan Detachment System; Him—Himalaya; Fm.—Formation; GHS—Greater Himalaya Sequence.

rocks through the ~350–60 °C temperature window (Reiners and Brandon, 2006).

AFT ages of bedrock samples range between 15.6 ± 2.8 Ma and 12.7 ± 1.5 Ma and are within error of each other, with a mean age of 14.8 ± 3.2 Ma (Fig. 2C; Table DR1), indicating rapid cooling during the middle Miocene. For some samples, these ages may represent a maximum due to low track densities/uranium concentrations. The few AHe ages are between ca. 16 and ca. 3 Ma and show no correlations with grain size or eU (Table DR2; cf. the Data Repository). The Rongbuk River detrital sample shows a distribution of white mica $^{40}Ar/^{39}Ar$ ages with a ca. 16 Ma peak, and AFT ages characterized by a single population at ca. 15 Ma; AFT ages from the Gyachung Chhu River show a detrital population at ca. 14 Ma (Fig. 2B). The $^{40}Ar/^{39}Ar$ and AFT cooling ages of bedrock and sand samples indicate that the STDS footwall north of Mount

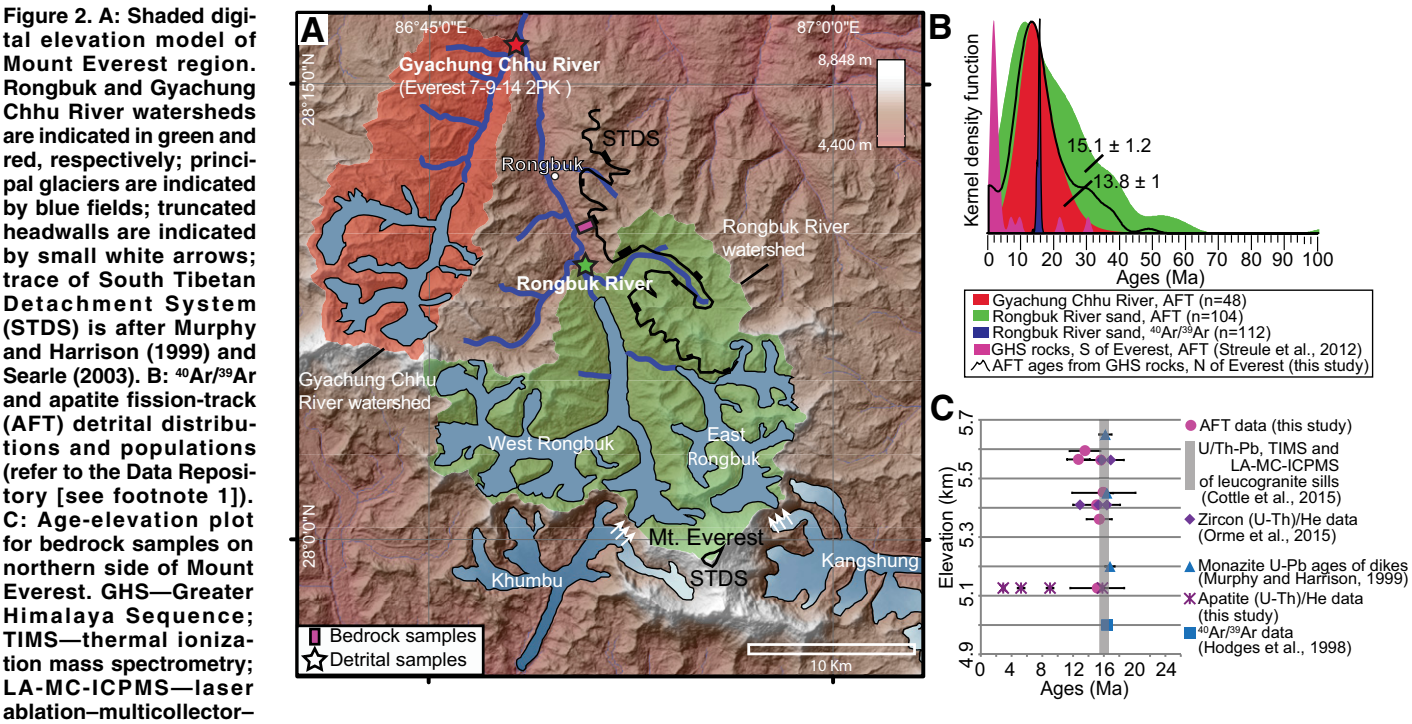

Figure 2. A: Shaded digital elevation model of Mount Everest region. Rongbuk and Gyachung Chhu River watersheds are indicated in green and red, respectively; principal glaciers are indicated by blue fields; truncated headwalls are indicated by small white arrows; trace of South Tibetan Detachment System (STDS) is after Murphy and Harrison (1999) and Searle (2003). B: $^{40}Ar/^{39}Ar$ and apatite fission-track (AFT) detrital distributions and populations (refer to the Data Repository [see footnote 1]). C: Age-elevation plot for bedrock samples on northern side of Mount Everest. GHS—Greater Himalaya Sequence; TIMS—thermal ionization mass spectrometry; LA-MC-ICPMS—laser ablation–multicollector–inductively coupled plasma–mass spectrometry.

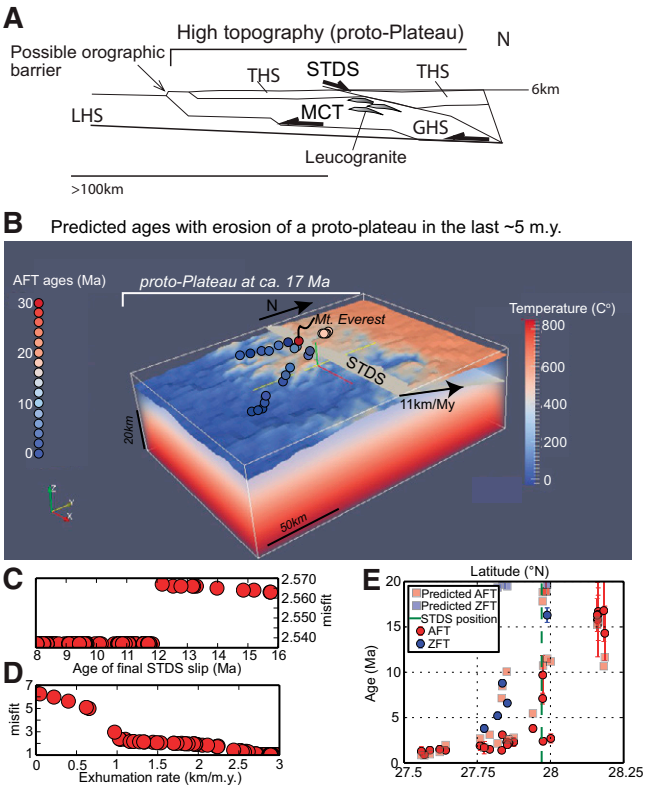

Figure 3. A: Schematic north-south structural profile showing a protoplateau extending southward to modern trace of Main Central Thrust (MCT) in eastern Nepal at ca. 17 Ma. LHS—Lesser Himalaya Sequence; THS—Tethyan Himalayan Sequence; STDS—South Tibetan Detachment System; GHS—Greater Himalaya Sequence. B: Predicted modeling ages (Pecube; Braun et al., 2012) for a scenario in which exhumation was localized near South Tibetan Detachment System (STDS) in mid-Miocene and was eroded in past 5–2 m.y.; dots represent observed ages colored by age (Ma). C: Timing of STDS activity as constrained by the model based on the misfit (the lower the misfit, the better the model; see the Data Repository [text footnote 1] for details). D: Exhumation rates of southern side of Mount Everest after 12 Ma. E: Latitude-age profile through Mount Everest with observations and best model predictions (RUN04). AFT—apatite fission-track; ZFT—zircon fission-track.

Everest cooled rapidly through the ~350–60 °C thermal window between ca. 16 and ca. 12 Ma.

EXHUMATION ACROSS MOUNT EVEREST AND THERMOKINEMATIC NUMERICAL MODELING

Comparison of our data with thermochronological ages from GHS rocks from roughly the same structural position across the orographic divide to the south (Streule et al., 2012) indicates asymmetric cooling and exhumation. GHS rocks north of Mount Everest and below the present STDS cooled rapidly through the $^{40}Ar/^{39}Ar$, zircon He, and AFT closure temperatures during early to middle Miocene time; a few Oligocene–early Miocene AFT ages (Streule et al., 2012; Sakai et al., 2005) can be explained by limited exhumation of STDS hanging-wall rocks. In contrast, data from GHS rocks exposed south of Mount Everest indicate that they cooled through the white mica $^{40}Ar/^{39}Ar$ closure temperature during Miocene time but remained hotter than the AFT closure temperature until they were exhumed during the Pliocene (Wang et al., 2010; Streule et al., 2012; Thiede and Ehlers, 2013; see the Data Repository, and Fig. DR1 therein). The asymmetric exhumation history of Mount Everest can be explained by localized tectonic exhumation along the STDS between ca. 16 and ca. 12 Ma. Limited erosion since ca. 12 Ma to the north of Mount Everest is consistent with high paleoelevations (Gébelin et al., 2013) and limited precipitation in a dry, plateau-like environment. GHS footwall rocks to the south of Mount Everest were instead exhumed largely to upper-crustal levels over the past ~5 m.y. Asymmetric exhumation is also supported by estimates of the volume of removed material inferred from calculations of AFT closure paleodepths (Fig. DR2).

We suggest that younger ages to the south of Mount Everest are the result of erosion of high paleotopography that extended farther south during the mid-Miocene (Fig. 3). In order to test this asymmetric tectono-topographic and erosional scenario, we used Pecube (Braun et al., 2012), a finite-element code that solves the three-dimensional (3-D) heat transport equation in a crustal block affected by vertical and/or horizontal advection with evolving topography (Fig. 3; cf. the Data Repository for details).

Present-day topography was inferred from the Shuttle Radar Topography Mission (SRTM) 90 m digital elevation model (DEM) version 4.1. The code incorporates the STDS as a low-angle, north-dipping normal fault. AFT ages from north of Mount Everest indicate STDS activity between 16 and 12 Ma. In the model, the hanging wall moves northward with respect to the footwall. We assume that at 17 Ma, relief similar to that observed today north of Mount Everest extended southward to the present trace of the MCT in eastern Nepal. For our best model, we imposed 10% of present-day relief on a mean altitude of ~5000 m in the region south of Mount Everest (Fig. 3A; Fig. DR4B), and then we progressively increased relief and lowered mean altitude starting at 5 Ma, according to details specified in the Data Repository.

This model of asymmetric exhumation produces results consistent with a protoplateau that began to be eroded between 5 and 2 Ma. A symmetric model, i.e. with no protoplateau erosion, cannot explain the observed ages (see the Data Repository). Inverse modeling following the method presented in Braun and Robert (2005) and Robert et al. (2011) for free parameters shows that (1) the STDS had to be active before ca. 12 Ma to explain the thermochronological data observed at Mount Everest (Fig. 3C), and (2) erosion south of Mount Everest (at rates of 1–3 mm/yr after 12 Ma; Fig. 3D) controlled the attainment of modern relief and is responsible for the younger ages observed on the southern side of the modern drainage divide.

IMPLICATIONS FOR TECTONIC AND TOPOGRAPHIC MODELS OF THE HIMALAYA

Our results have implications for tectonic models of the Himalayan orogenic system. The wedge-fault model of Yin (2006) proposes that the STDS originated as a north-verging passive back thrust above the GHS rocks and is connected to the north-verging Great Counter Thrust (GCT) along the India-Asia suture zone. This requires simultaneous slip on the STDS and thrust burial of rocks in the Everest region, as well as in the footwall of the GCT. Results presented here, and those of Carrapa et al. (2014) from the rocks in the footwall of the GCT, indicate regional cooling, rather than burial heating, during early to mid-Miocene time. This argues against a connection between the GCT and the STDS at that time. The popular channel flow model proposes that GHS rocks (including those forming the bulk of Mount Everest) were extruded southward from beneath the Tibetan Plateau in a viscous channel bounded by the STDS at the top and the MCT at the bottom. This model couples climate-driven erosion and young and rapid exhumation (<6 Ma at rates up to 10 mm/yr; Jamieson et al., 2004) of GHS rocks within the channel. We note that the MCT and its hanging-wall rocks (GHS) have been structurally and erosionally breached by growth of a large duplex in underlying Lesser Himalayan rocks beginning at ca. 11–10 Ma, some 10 m.y. after formation of the MCT and STDS (e.g., Robinson and Pearson, 2006). Accordingly, the relatively steep northward (30–45°N) dip of the MCT along the south flank of the modern High Himalaya was produced by passive northward tilting above the Lesser Himalayan duplex, rather than by steep, surfaceward advection of GHS rocks while the MCT and STDS were active in early Miocene time. If

such advection did occur, it must have taken place farther south, near the front of the modern Himalaya along the original trace of the MCT. Coupled with our results, this indicates that the STDS has been localized to its present location since the early Miocene. We suggest that during the Miocene, an elevated area similar to modern Tibet extended south into Nepal (Fig. 3A); the orographic barrier at that time was farther south and has migrated to its modern position over the past ~5 m.y. as a result of erosion.

ACKNOWLEDGMENTS

This research was funded by the National Science Foundation (grants EAR 1008527 and 1140068). We thank James Spotila, Laura Webb, and two anonymous reviewers for constructive criticisms, Jo-Anne Wartho for help with $^{40}Ar/^{39}Ar$ analyses, Ryan Leary and Pete Lippert for help with fieldwork, Paul Kapp for scientific exchange, and Kip Hodges for stimulating discussions.

REFERENCES CITED

Aikman, A.B., Harrison, T.M., and Ding, L., 2008, Evidence for early (>44 Ma) Himalayan crustal thickening, Tethyan Himalaya, southeastern Tibet: Earth and Planetary Science Letters, v. 274, p. 14–23, doi:10.1016/j.epsl.2008.06.038.

Beaumont, C., Jamieson, R.A., Nguyen, M.H., and Medvedev, S., 2004, Crustal channel flows: 1. Numerical models with applications to the tectonics of the Himalayan-Tibetan orogen: Journal of Geophysical Research, v. 109, p. B06406, doi:10.1029/2003JB002809.

Bookhagen, B., and Burbank, D.W., 2006, Topography, relief, and TRMM-derived rainfall variations along the Himalaya: Geophysical Research Letters, v. 33, p. L08405, doi:10.1029/2006GL026037.

Braun, J., and Robert, X., 2005, Constraints on the rate of post-orogenic erosional decay from low-temperature thermochronological data: Application to the Dabie Shan, China: Earth Surface Processes and Landforms, v. 30, p. 1203–1225, doi:10.1002/esp.1271.

Braun, J., et al., 2012, Quantifying rates of landscape evolution and tectonic processes by thermochronology and numerical modeling of crustal heat transport using PECUBE: Tectonophysics, v. 524, p. 1–28, doi:10.1016/j.tecto.2011.12.035.

Burchfiel, B.C., Zhiliang, C., Hodges, K.V., Yuping, L., Royden, L.H., Changrong, D., and Jiene, X., 1992, The South Tibetan Detachment System, Himalayan Orogen: Extension Contemporaneous With and Parallel To Shortening in a Collisional Mountain Belt: Geological Society of America Special Paper 269, 41 p., doi:10.1130/SPE269-p1.

Burg, J., Brunel, M., Gapais, D., Chen, G., and Liu, G., 1984, Deformation of leucogranites of the crystalline Main Central Sheet in southern Tibet (China): Journal of Structural Geology, v. 6, p. 535–542, doi:10.1016/0191-8141(84)90063-4.

Carrapa, B., Orme, D.A., DeCelles, P.G., Kapp, P., Cosca, M.A., and Waldrip, R., 2014, Miocene burial and exhumation of the India-Asia collision zone in southern Tibet: Response to slab dynamics and erosion: Geology, v. 42, p. 443–446, doi:10.1130/G35350.1.

Cottle, J.M., Searle, M.O., Jessup, M., Crowley, J.L., and Law, R.D., 2015, Rongbuk re-visited: Geochronology of leucogranites in the footwall of the South Tibetan detachment system, Everest region, southern Tibet: Lithos, v. 227, p. 94–106, doi:10.1016/j.lithos.2015.03.019.

Gébelin, A., Mulch, A., Teyssier, C., Jessup, M.J., Law, R.D., and Brunel, M., 2013, The Miocene elevation of Mount Everest: Geology, v. 41, p. 799–802, doi:10.1130/G34331.1.

Harris, N., and Massey, J., 1994, Decompression and anatexis of Himalayan metapelites: Tectonics, v. 13, p. 1537–1546, doi:10.1029/94TC01611.

Hodges, K., 2000, Tectonics of the Himalaya and southern Tibet from two perspectives: Geological Society of America Bulletin, v. 112, p. 324–350.

Hodges, K., Bowring, S., Davidek, K., Hawkins, D., and Krol, M., 1998, Evidence for rapid displacement on Himalayan normal faults and the importance of tectonic denudation in the evolution of mountain ranges: Geology, v. 26, p. 483–486, doi:10.1130/0091-7613(1998)026<0483:EFRDOH>2.3.CO;2.

Jamieson, R., Beaumont, C., Medvev, S., and Nguyen, M.H., 2004, Crustal channel flows: 2. Numerical models with implications for metamorphism in the Himalayan-Tibetan orogen: Journal of Geophysical Research, v. 109, p. B06407, doi:10.1029/2003JB002811.

Murphy, M., 2007, Isotopic characteristics of the Gurla Mandhata metamorphic core complex: Implications for the architecture of the Himalayan orogeny: Geology, v. 35, p. 983–986, doi:10.1130/G23774A.1.

Murphy, M.A., and Harrison, T.M., 1999, Relationship between leucogranites and the Qomolangma detachment in the Rongbuk Valley, south Tibet: Geology, v. 27, p. 831–834, doi:10.1130/0091-7613(1999)027<0831:RBLATQ>2.3.CO;2.

Orme, D.A., Reiners, P.W., Hourigan, J.K., and Carrapa, B., 2015, Effects of inherited cores and magmatic overgrowths on zircon (U-Th)/He ages and age-eU trend from Greater Himalayan sequence rocks, Mount Everest region, Tibet: Geochemistry Geophysics Geosystems, v. 16, p. 2499–2507, doi:10.1002/2015GC005818.

Owen, L.A., Robinson, R., Benn, D.I., Finkel, R.C., Davis, N.K., Yi, C.-L., Putkonen, J., Li, D.-W., and Murray, A.S., 2009, Quaternary glaciation of Mount Everest: Quaternary Science Reviews, v. 28, p. 1412–1433, doi:10.1016/j.quascirev.2009.02.010.

Pêcher, A., 1991, The contact between the Higher Himalaya Crystallines and the Tibetan Sedimentary Series: Miocene large-scale dextral shearing: Tectonics, v. 10, p. 587–598, doi:10.1029/90TC02655.

Reiners, P.W., and Brandon, M.T., 2006, Using thermochronology to understand orogenic erosion: Annual Review of Earth and Planetary Sciences, v. 34, p. 419–466, doi:10.1146/annurev.earth.34.031405.125202.

Robert, X., van der Beek, P., Braun, J., Perry, C., and Mugnier, J.-L., 2011, Control of detachment geometry on lateral variations in exhumation rates in the Himalaya: Insights from low-temperature thermochronology and numerical modeling: Journal of Geophysical Research, v. 116, p. B05202, doi:10.1029/2010JB007893.

Robinson, D., and Pearson, O., 2006, Exhumation of Greater Himalayan rock along the Main Central thrust in Nepal: Implications for channel flow, *in* Law, R.D., Searle, M.P., and Godin, L., eds., Channel Flow, Ductile Extrusion, and Exhumation in Continental Collision Zones: Geological Society of London Special Publication 268, p. 255–267, doi:10.1144/GSL.SP.2006.268.01.12.

Sakai, H., Sawada, M., Takigami, Y., Orihashi, Y., Danhara, T., Iwano, H., Kuwahara, Y., Dong, Q., Cai, H., and Li, J., 2005, Geology of the summit limestone of Mount Qomolangma (Everest) and cooling history of the Yellow Band under the Qomolangma detachment: The Island Arc, v. 14, p. 297–310, doi:10.1111/j.1440-1738.2005.00499.x.

Scherler, D., Bookhagen, B., and Strecker, M.R., 2011, Spatially variable response of Himalayan glaciers to climate change affected by debris cover: Nature Geoscience, v. 4, p. 156–159, doi:10.1038/ngeo1068.

Searle, M., 2003, Geological Map of the Mount Everest–Makalu Region, Nepal–South Tibet Himalaya: Oxford, UK, Oxford University, scale 1:100,000.

Streule, M.J., Carter, A., Searle, M.P., and Cottle, J.M., 2012, Constraints on brittle field exhumation of the Everest-Makalu section of the Greater Himalayan Sequence: Implications for models of crustal flow: Tectonics, v. 31, p. TC3010, doi:10.1029/2011TC003062.

Thiede, R.C., and Ehlers, T.A., 2013, Large spatial and temporal variations in Himalayan denudation: Earth and Planetary Science Letters, v. 371–372, p. 278–293, doi:10.1016/j.epsl.2013.03.004.

Wang, A., Garver, J.I., Wang, C., Smith, J.A., and Zhang, K., 2010, Episodic exhumation of the Greater Himalayan Sequence since the Miocene constrained by fission track thermochronology in Nyalam, central Himalaya: Tectonophysics, v. 495, p. 315–323, doi:10.1016/j.tecto.2010.09.037.

Yin, A., 2006, Cenozoic tectonic evolution of the Himalayan orogen as constrained by along-strike variation of structural geometry, exhumation history, and foreland sedimentation: Earth-Science Reviews, v. 76, p. 1–131, doi:10.1016/j.earscirev.2005.05.004.

Manuscript received 3 February 2016
Revised manuscript received 31 May 2016
Manuscript accepted 3 June 2016

Printed in USA